Investigation of the far field pressure pulse generated by vortex-wedge interaction using Howe's acoustic analogy

Marios I Spiropoulos, Florent Margnat, Vincent Valeau, Peter Jordan

AIAA AVIATION Forum
12-16 June 2023, San Diego, CA and Online
AIAA AVIATION 2023 Forum

10.2514/6.2023-4514

Investigation of the far field pressure pulse generated by vortex-wedge interaction using Howe's acoustic analogy

Marios I. Spiropoulos*, Florent Margnat †, Vincent Valeau ‡, Peter Jordan §
Institut PPRIME UPR 3346, CNRS - Université de Poitiers - ISAE ENSMA, Poitiers 86022, France

The far field generated sound by a vortex interacting with a semi-infinite rigid wedge is studied in the time domain. The theory of vortex sound is used to calculate the far field sound, under the assumption that the distance between the aerodynamic source and the edge of the wedge is acoustically compact ($k\,|\vec{y}_0| << 1$). Analytical expressions are presented for different cases: i) The self induction of a point vortex around the wedge, ii) the convection effects induced by the free stream flow with velocity U and angle of attack η and iii) regions with a Gaussian distribution of vorticity. The presented models are compared with existing solutions in the literature, and conclusions regarding the physics of the problem are drawn.

I. Introduction

Air-frame noise is one of the principal components of aircraft noise emission, especially during landing. It is generated by the interaction of the flow with the aircraft's structure. The main sources of air-frame noise on an aircraft are the landing gear, the leading, trailing edges of the airfoils and regions with cavities [1]. The aerodynamic sound produced by turbulence-airfoil interactions has been extensively studied by detailed numerical simulations, experiments and analytical methods. An exhaustive review of trailing edge noise is presented by Lee et al. (2021) [2]. Despite the fact that approximate analytical solutions lack the accuracy of high-fidelity numerical simulations, they provide simple models which enhance the understanding of the physics of the problem. Analytical models based on Lighthill's acoustic analogy [3] and the work of Curle (1955), Ffowcs Wiliams and Hawkings (1969) ([4] , [5]) or the theory of Vortex Sound ([6], [7]) have been developed in order to shed light on the mechanism of aerodynamic noise generation of wall bounded flows. Ffowcs Williams and Hall (1970) [8] applied Lighthill's theory to show that quadrupole sources close to an edge of a semi-infinite half plane lead to an acoustic intensity that scales with the fifth power of the turbulent velocity. Crighton and Leppington (1971) calculated scaling laws for quadruple and dipole sources for soft and hard wedge-like objects by considering that the Green's function of a compact object can be obtained as the solution of the Laplace equation when the observer is many wavelengths away and the dimensions of the obstacle immersed in the flow is acoustically compact [9]. Crighton (1972) examined the aerodynamic sound generated by a line vortex with its axis parallel to the edge of a semi-infinite rigid half plane [10]. Howe (1975a) [7], (1975b) [11], by introducing the concept of compact Green's functions, extended this idea to two dimensional problems in the time domain and obtained simple closed form analytical solutions that clarify the physical mechanisms underpinning aerodynamic sound generation [12], [13]. Kambe et al. (1985) [14] solved the problem of a vortex passing very close to the edge of semi-infinite half plane by assuming that the vortex path is not influenced by the existence of the edge. The results were verified also experimentally and an extension of this work was proposed by Chang and Chen (1994) [15]. Priddin et al. (2018) illustrated that simplified models derived in the framework of theory of vortex sound can be extended to investigate methods for controlling actively and passively the trailing edge noise [16].

In the present work the theory of vortex sound is employed to study the ideal problem of turbulent fluctuations, modelled as point vortices, impinging on a semi-infinite rigid wedge. In section II the simplified model, proposed by Howe (2002) [17], that describes the sound generation by a point vortex passing by the edge of a rigid semi-infinite half plane is reviewed. In section III, this model is extended to wedges with arbitrary angles. In subsection III.B, the proposed model is further generalised by considering the convection of the point vortex by mean velocity of the free stream. It is shown that the vortex trajectory and the far-field acoustic pressure pulse are influenced by a non-dimensional number called the wedge-deflection strength. Finally the effect of viscosity on the far-field pressure pulse is examined in Section IV.

*Graduate Student,marios.spiropoulos@univ-poitiers.fr
†Assistant Professor, florent.margnat@univ-poitiers.fr
‡Professor, vincent.valeau@univ-poitiers.fr
§Research Director, peter.jordan@univ-poitiers.fr

II. Edge-Vortex Interaction: Howe's Half plane problem

The turbulent fluctuations around the edge of a semi-infinite rigid plate ($x_1 < 0, x_2 = 0$) is modelled as a single line vortex, shown in Fig. 1. It is assumed that the acoustic wavelength λ is much larger than the closest distance l between the edge and the vortex. Any effect of the freestream flow is omitted and the point vortex is self induced around the edge of the half plane. Howe's theory of vortex sound is applied to obtain the pressure pulse in the far field.

$$p\left(\vec{x},t\right) = -\int_t \int_V \left(\vec{\omega}\times\vec{v}\right)\left(\vec{y},t\right)\vec{\nabla}G\left(\vec{x},\vec{y},t-\tau\right)dy^3dt \tag{1}$$

where the source term $\vec{\omega}\times\vec{v}$ is the Lamb vector and G denotes the Green function. Howe showed that for two-dimensional sources close to the edge, the time-domain compact Green's function for the diffraction field around a half plane [7] can be written as

$$G \approx \frac{\phi^*\left(\vec{x}\right)\phi^*\left(\vec{y_0}\right)}{\pi|\vec{x}|}\delta\left(t-\tau\right), |\vec{x}| \to \infty \tag{2}$$

where $\vec{x} = (x_1, x_2)$ denotes the coordinates of the observer in the far field, such that $k|\vec{x}| >> 1$ and $\vec{y_0} = \left(y_{0_1}, y_{0_2}\right)$ corresponds to the coordinates of the vortex, which is located close to the edge of the semi-infinite half plane, such that $k|\vec{y_0}| << 1$. ϕ^* represents the velocity potential of the incompressible, irrotational flow around the edge of the half plane in the absence of any vortex and $\tau = t - |\vec{x}|/c_0$ corresponds to the retarded time. Expanding the source term yields:

$$\vec{\omega}\times\vec{v} = \Gamma\hat{x}_3 \times \frac{d\vec{y}}{dt}\delta\left(\vec{y}-\vec{y_0}\left(t\right)\right) \tag{3}$$

From here on, the polar coordinate system will be used: i) $\vec{x} = r\left(\cos\theta, \sin\theta\right)$ and ii) $\vec{y_0} = r_0\left(\cos\theta_0, \sin\theta_0\right)$ unless stated otherwise. Substituting Equations (2), (3) into (1) the pressure pulse in the far field can be written form,

$$p\left(\vec{x},\tau\right) = \frac{\rho_0\Gamma\sin\left(\theta/2\right)}{\pi\sqrt{r}}\left[\frac{d\vec{y_0}}{d\tau}\cdot\vec{\nabla}\Psi^*\right]\left(\vec{y_0}\right), \tag{4}$$

where Ψ^* is the stream-function of the potential flow ($\phi^*\left(\vec{y_0}\right)$) around the edge of a half-plane when no vortices are present. The operator $\frac{D}{D\tau}$ corresponds to the material derivative with respect to the vortex trajectory. For 2-D flows we can write (cartesian coordinates for simplicity)

$$\frac{d\vec{y_0}}{d\tau}\cdot\nabla\Psi^* = \frac{dy_{01}}{d\tau}\frac{d\Psi^*}{dy_{01}} + \frac{dy_{02}}{d\tau}\frac{d\Psi^*}{dy_{02}} = \frac{D\Psi^*}{D\tau}\left(\vec{y_0}\right),$$

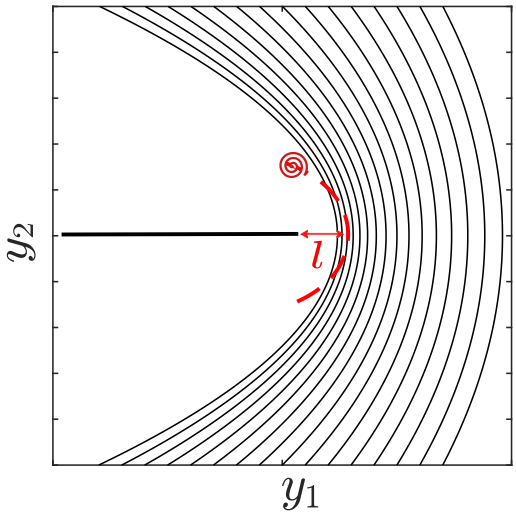

Fig. 1 Two-Dimensional Problem: Interaction of line vortex (blue dot) with semi-infinite half plane. The red-dashed line corresponds to the vortex trajectory, due to the interaction with its image point, while the black solid lines are the streamlines (Ψ^*) in the absence of any vortex.

One of the main results of this ideal problem is that it enables the following physical interpretation regarding the mechanism of sound generation. The noise in the far field is generated when the vortex path crosses the streamlines, given by Ψ^*. Vortices that follow these streamlines do not produce sound. For example a vortex far from the edge travels with an equivalent velocity $U = \Gamma/(8\pi l)$, parallel to those streamlines and no sound is produced [12],[13],[7].

$D\Psi^*/D\tau$ is deduced from the vortex path, which is obtained by taking into account the presence of the vortex around the half-plane and its image point, details shown in [13]. In the present problem, it is given by the velocity potential flow of a vortex and its image close to a semi-infinite half plane. Then, it yields

$$p\left(\vec{x},\tau\right) = \frac{\rho_0\Gamma^2\sin\left(\theta/2\right)}{\left(4\pi l\right)^2}\sqrt{\frac{l}{r}}\left[\frac{\Gamma\tau/\left(8\pi l^2\right)}{\left[1+\left(\Gamma\tau/\left(8\pi l^2\right)\right)^2\right]^{5/4}}\right], \tag{5}$$

Kambe et al. [14] studied the same problem experimentally and theoretically, by applying the theory of vortex sound, using the inverse-Fourier-transformed asymptotic forms for low frequencies of the Green functions for half-plane scattering. Kambe's method is more accurate since it is based on the exact Green function, however due to the higher mathematical complexity of that approach it is not easy to develop a closed form analytical solution as in Eq. (5) and study the physics of the problem more closely. Furthermore, the work of Kambe et al. was restricted to vortices purely convected by the mean flow while the bending of the vortex path close to the edge was not taken into account.

III. Semi Infinite Wedge-problem

The results of Section II will now be generalised for any arbitrary wedge with half angle Ω. Figure 2 depicts the geometry of the problem. The wedge parameter $\gamma = 2\left(\pi-\Omega\right)/\pi$ is introduced and ranges from $\gamma = 2$ which corresponds to the limiting case of a half plane (very sharp edge) to $\gamma = 1$ (infinite wall). The physical space is restricted from the lower to the upper face of the wedge, $\theta_0 \in [-\gamma\pi/2, \gamma\pi/2]$. It should be noted that for $\gamma < 1$ the problem resembles rather the aerodynamic sound generated by a closed triangular cavity, which is not the subject of the present study. Following Howe's methodology [13], the complex velocity potential close to the edge is given by:

$$W\left(z_j\right) = -iz_j^{1/\gamma} = -ir_j^{1/\gamma}\left(\cos\left(\theta_j/\gamma\right) + i\sin\left(\theta_j/\gamma\right)\right), \tag{6}$$

here r_j, θ_j denote source or receiver coordinates, $\phi^* = Re\left[-iW\left(z_j\right)\right]$ and $\Psi^* = Im\left[-iW\left(z_j\right)\right]$ [13]. Combining Eqs.(1), (2), (3) one obtains:

$$p\left(r,\theta,\tau\right) = \frac{\rho_0\Gamma\sin\left(\theta/\gamma\right)}{\pi r^{\frac{\gamma-1}{\gamma}}}\left[-\frac{r_0^{1/\gamma-1}}{\gamma}\frac{dr_0}{d\tau}\cos\left(\theta_0/\gamma\right) + \frac{r_0^{1/\gamma}}{\gamma}\sin\left(\theta_0/\gamma\right)\frac{d\theta_0}{d\tau}\right] \tag{7}$$

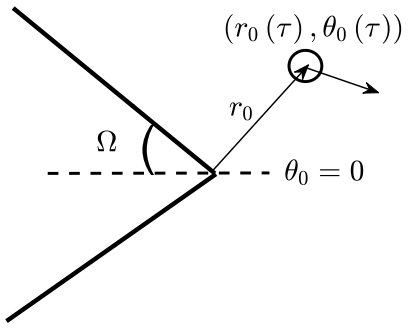

Fig. 2 Geometry of the wedge problem.

Chang and Chen [15] using the same analysis presented by Kambe et al (1985), derived a similar expression for the far field pressure pulse, by using the low-frequency asymptotic expansion of the Green's function for wedge scattering. This analysis was also restricted to cases where the edge effect is omitted.

A. Self induced vortex around the edge of a wedge

A single point vortex is first considered in the vicinity of the edge of a semi-infinite wedge and the free-stream flow is ignored. The equations of motion can be obtained by the following expression according to [13]

$$\frac{dz_0^*}{dt} = -i\frac{\Gamma\zeta''(z_0)}{4\pi\zeta'(z_0)} + F'(z_0) \tag{8}$$

where z_0 is the position of the vortex core in the complex plane, z_0^* the complex conjugate of z_0, $\zeta(z_0)$ is the conformal mapping of z_0 in the ζ-plane and $F(z_0)$ a regular function of z_0. Since the convection of the vortex core is not considered, we may write

$$F(z_0) = \frac{i\Gamma}{2\pi}\ln\left(\zeta(z) - \zeta^*(z_0)\right),$$

which corresponds to the velocity field induced by an image vortex. To account for the presence of a corner the following conformal transform is applied

$$\zeta(z) = iz^{1/\gamma}.$$

Using the polar form of the complex number, $z = re^{i\theta}$, Eq.(8) results in a 2×2 system of non-linear differential equations of first order. The vortex position at any time instant is then given by

$$\begin{aligned} r_0 &= l\sqrt{1 + (2\tilde{\tau}/\gamma)^2}, \\ \theta_0 &= \gamma\tan^{-1}\left(-2\tilde{\tau}/\gamma\right), \end{aligned} \tag{9}$$

where $\tilde{\tau} = \frac{\Gamma\tau}{8\pi l^2}$ is a non dimensional time parameter and l denotes the closest distance from the vortex to the edge. Full steps of the derivation are shown in Appendix A. Substituting Eq.(9) into Eq.(7) we obtain the expression for the far-field pressure pulse which can be written as the product of two parameters, one factor that is mainly constant and contains the amplitude and directivity and a function that depends on time and the wedge angle T_{wedge}.

$$p(\vec{x}, \tau) = CT_{wedge}$$

$$\begin{aligned} C &= \frac{\rho_0\Gamma^2}{8\pi^2 l^2}\sin(\theta/\gamma), \\ T_{wedge} &= 2\frac{(rl)^{1/\gamma}}{r}\left(\frac{\gamma-1}{\gamma^2}\right)\left[\frac{2\tilde{\tau}/\gamma}{\left[1 + (2\tilde{\tau}/\gamma)^2\right]^{\frac{3\gamma-1}{2\gamma}}}\right] \end{aligned} \tag{10}$$

Equation (10) is a more general version of Eq.(5) since it contains an arbitrary wedge angle. Indeed, for $\gamma = 2$ one obtains Eq.(5). It can be seen that the wedge angle influences the vortex path and thus the far-field pressure. In the limiting case of $\gamma = 1$ (infinite wall), the vortex path is parallel to the stream lines of the hypothetical potential flow, thus Eq.(10) yields $p = 0$. The pressure pulse is mainly dependent on the time-wedge function $T_{wedge}(\tau, \gamma)$, since the amplitude is constant and the directivity function $(\sin(\theta/\gamma))$ takes values from -1 to 1. It is shown in Fig. 3 that for non-dimensional time units close to zero, the wedge angle does not have a strong influence on the pressure signature since T_{wedge} grows linearly with time. However, it seems that the pressure pulse tends to decrease as the wedge angle increases. By examining the behaviour of the time-wedge function, it can be shown that the maximum value of each pressure pulse depends explicitly on the wedge angle. The maxima are found by,

$$\frac{\partial T_{wedge}}{\partial\tilde{\tau}} = 0$$

and the non-dimensional time when acoustic radiation peak occurs yields,

$$\tilde{\tau}^* = (\gamma/2)\sqrt{\frac{\gamma}{2\gamma - 1}} \tag{11}$$

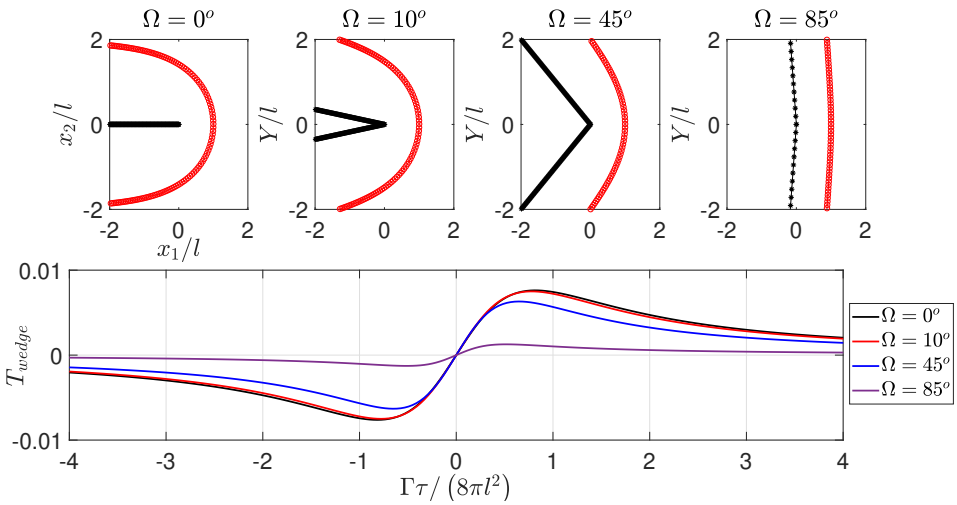

Fig. 3 Pressure pulses in the far field for different wedge angles. The closest distance from the edge is chosen to be $l = 0.025m$, and the circulation of the vortex $\Gamma = 28m^2/s$

Substituting Equation (11) into Eq.(10), it follows that the maxima of the pressure pulse are obtained by,

$$T_{wedge,max} = 2\frac{(rl)^{1/\gamma}}{r}\left(\frac{\gamma-1}{\gamma^2}\right)\left[\frac{\sqrt{\frac{\gamma}{2\gamma-1}}}{\left[1+\frac{\gamma}{2\gamma-1}\right]^{\frac{3\gamma-1}{2\gamma}}}\right]. \tag{12}$$

Figure 4 depicts the trends of the maxima of the far field pressure pulses (Eq.(12)) for $\Omega \in [0, 90°]$. As a result, the present model indicates that large wedge angles generate less sound in the far field when the source distance is acoustically compact ($kr_0 << 1$).

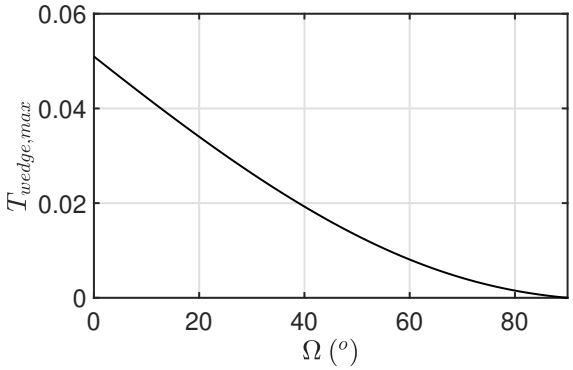

Fig. 4 Maximum values of T_{wedge} with respect to the wedge angle, obtained by Eq.(12)

One can extract more information regarding the time evolution of the pressure pulse by examining Eq.(11). Solving for the dimensional time τ^* that corresponds to the maximum amplitude yields,

$$\tau^* = \frac{4\pi l^2}{\Gamma}\gamma\sqrt{\frac{\gamma}{2\gamma-1}}. \tag{13}$$

The time of the maximum radiation peak thus depends on i) the circulation ii) distance from the edge and iii) the wedge angle. For sources closer to the edge and/or vortices with strong circulation τ^* decreases and thus the radiation peak occurs sooner. Furthermore, τ^* decreases further as the wedge angle increases. This can be seen also in Fig. 3. For

vortices with the same circulation and distance from the edge the peak of radiation that corresponds to a wedge angle of $\Omega = 45^o$ (blue line) happens sooner than the one of the half plane (black line). Since at large times the pressure amplitude decreases significantly, it will be shown that most of the acoustic energy is radiated at the time interval $[0, \kappa\tau^*]$, where $\kappa\tau^*$ is the total time when most of the acoustic energy is radiated to the far field. Thus, the time of maximum sound radiation is expressed as

$$\Delta t_{rad} = \kappa \sqrt{\left(\frac{4\pi\gamma l^2}{2\Gamma}\right)^2 \frac{\gamma}{2\gamma - 1}}, \tag{14}$$

From Eq.(14) it can be easily deduced that the time radiation of the half plane is the longest compared to the other wedges. This will be illustrated by considering the following example. Maximum radiation time obtained for a half plane ($\Omega = 0^o$) is compared to that of a wedge with $\Omega = 25^o$, for the same flow conditions. Suppose that $\kappa = 3.5$, then the results are shown in Fig. 5. Indeed the time radiation of the wedge ($\Omega = 25^o$) is shorter than that of the half-plane.

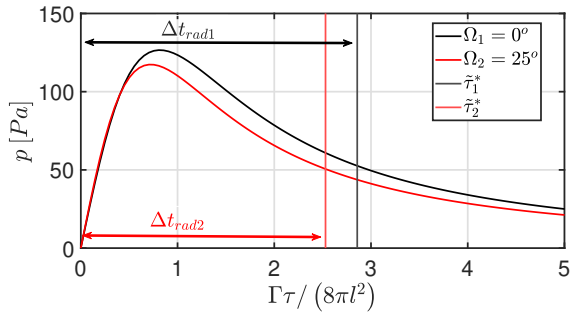

Fig. 5 Comparison of radiation times between a half plane (black line) and a wedge angle of 25^0 (red line). The results are shown for $l = 0.025m$, $\Gamma = 28m^2/s$ and an observer in the far field $r = 25m$, $\theta = \pi$.

It is also noted that the area under the curve in the interval $[0, \Delta t_{rad}]$ is larger for the half plane. Therefore, it can be concluded that less sharp wedges tend to radiate most of the acoustic energy faster, while the amount of radiated acoustic energy becomes maximum when $\gamma = 2$.

Another point of interest is the asymptotic behaviour of the far field pressure for short and large non-dimensional times. For short non-dimensional times, that is $2\tilde{\tau}/\gamma << 1$ the pressure pulse yields

$$p_{short} = \frac{(rl)^{1/\gamma}}{r} \frac{\rho_0 \Gamma^2}{2\pi^2 l^2} \sin(\theta/\gamma) \left(\frac{\gamma - 1}{\gamma^3}\right) \tilde{\tau}, \tag{15}$$

and it depends linearly on $\tilde{\tau}$. However for $2\tilde{\tau}/\gamma >> 1$:

$$p_{large} = \frac{\rho_0 \Gamma^2}{8\pi^2 l^2} \sin(\theta/\gamma)\, 2 \frac{(rl)^{1/\gamma}}{r} \left(\frac{\gamma - 1}{\gamma^2}\right) \left(\frac{2\tilde{\tau}}{\gamma}\right)^{\frac{1-2\gamma}{\gamma}}. \tag{16}$$

It can be observed that for $\Omega \in [0, 90°]$, p_{large} has the least contribution to the far field sound. Suppose that the turbulence around the edge is modeled as a vortex with a circulation given by $\Gamma = 2\pi v R$, where R the radius and v a measure of the velocity fluctuation. Then the time scale can be approximated as $\tau = l/v$. It yields

$$\frac{2\Gamma\tau}{8\pi l^2 \gamma} = \frac{1}{2\gamma}\left(\frac{R}{l}\right).$$

Thus, the asymptotic expressions can be reformulated in order to derive the following scaling laws.

$$\begin{aligned} p_{short} &\sim v^2 l^{\frac{1-3\gamma}{\gamma}} R^3, \quad R/l << 1 \\ p_{large} &\sim v^2 R^{1/\gamma}, \quad R/l >> 1 \end{aligned} \tag{17}$$

Kambe et al. (1985) showed experimentally that vortices passing near a semi-infinite plate, with $R/l << 1$ follow a scaling law $v^{2.53}l^{-2.24}$. For $\gamma = 2$ the asymptotic expresion of Eq.(17) gives $p \sim v^2 l^{-2.5}$. Chang and Chen [15] mention that the dependence of the acoustic intensity on the shortest distance l should not be influenced by the wedge angle. However, the results of Eq. (10) illustrates that the pressure scales as $\sim l^{(1-2\gamma)/\gamma}$, which agrees with the results of the scaling to a factor of $l^{-3/2}$ obtained by Ffowcs Williams and Hall [8] for the infinite plate, when $\gamma = 2$. As a result, it seems that the velocity scaling is mainly affected by the scattering of the surface (choice of Green's function) while the influence of the distance l seems to depend on the choice of the flow model close to the edge of the wedge.

Although the model presented in this section corresponds to an ideal case and lacks the accuracy and rigor of other existing models in the literature, it provides some physical insight about the important parameters that influence sound generation by flow around wedges. It is shown that the distance between the aerodynamic source and the edge influences the sound in the far field. The models presented in [15],[14] assume that the vortex is sufficiently far from the edge so that edge effects are not important. However, in the case of the half plane, the scaling law obtained experimentally in [14] lies between the theoretical results of their study (l^{-2}) and those presented here ($l^{-2.5}$). This indicates that even for vortex rings with a radius smaller than the distance from the edge, the edge effect does not vanish. It was also shown that as the wedge angle increases, the far field noise is generated faster, while the smaller the wedge angle the more acoustic energy is radiated in the far field. Moreover, the fact that peak radiation occurs sooner implies that in the frequency domain, larger wedge angles are expected to present peaks at higher frequencies.

B. Taking into account the convection of the vortex

In more realistic situations, turbulent fluctuations are influenced by convection effects of the mean flow. In this subsection, an attempt is made to generalise the previous model and take into account a combination of the phenomena that occur due to the proximity to the edge and convection. Furthermore, the aim of the following approach is to study the key parameters that influence the vortex trajectory close to the edge and whether they affect the far-field sound generation.

Let a line vortex in a free steam, with velocity U and an angle η with the horizontal axis, pass by the edge of a semi-infinite wedge. Since the problem becomes more complicated, we cannot now a priori the closest distance to the edge as in Eq. (9). However, we introduce the length scale l, which is a measure of the proximity of the vortex to the edge at the first time instants (Fig. 6). Equation (8) will be used as in subsection III.A to obtain the kinematics of

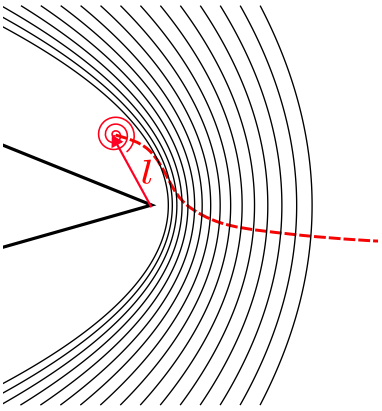

Fig. 6 Motion of a vortex close to the edge by taking into account convection effects. The red-dashed line corresponds to the vortex trajectory and l is a measure of its initial distance from the edge. The black solid lines correspond to the stream-function obtained by the potential flow around a wedge, in absence of vortices and convection effects, as shown in sub-section III.A.

the point vortex. The convection of the vortex core is taken into account by adding the free stream complex velocity potential to the induced velocity potential by the image vortex.

$$F(z_0) = \frac{i\Gamma}{2\pi} ln\left(\zeta(z) - \zeta^*(z_0)\right) + U z_0 e^{-i\eta}. \tag{18}$$

This results in a flow model with two velocity scales: one that corresponds to the free stream flow U and one that can be

considered as a turbulent fluctuation, such that $v \sim \Gamma/l$. By performing the same calculations as in subsection III.A we obtain:

$$\begin{pmatrix} \cos\theta_0 & -r_0\sin\theta_0 \\ \sin\theta_0 & r_0\cos\theta_0 \end{pmatrix} \frac{d}{d\tau}\begin{pmatrix} r_0 \\ \theta_0 \end{pmatrix} = \begin{pmatrix} \frac{\Gamma(\gamma-1)}{4\pi\gamma r_0}\sin\theta_0 + \frac{\Gamma}{4\pi\gamma r_0}\frac{\sin\left(\theta_0\frac{\gamma-1}{\gamma}\right)}{\cos(\theta_0/\gamma)} + U\cos\eta \\ \frac{-\Gamma(\gamma-1)}{4\pi\gamma r_0}\cos\theta_0 - \frac{\Gamma}{4\pi\gamma r_0}\frac{\cos\left(\theta_0\frac{\gamma-1}{\gamma}\right)}{\cos(\theta_0/\gamma)} + U\sin\eta \end{pmatrix}. \tag{19}$$

The system of Equation (19) is solved with the method of determinants and the trajectory of the vortex is described by the following coupled system of differential equations.

$$\begin{aligned} \dot{r_0} &= -\frac{\Gamma}{4\pi\gamma r_0}\tan(\theta_0/\gamma) + U\cos(\theta_0-\eta), \\ \dot{\theta}_0 &= -\frac{\Gamma}{4\pi r_0^2} - \frac{U}{r_0}\sin(\theta_0-\eta), \end{aligned} \tag{20}$$

where $(\dot{f})$ denotes the first time derivative of the function f. The system of Eqs. (20) cannot be solved analytically, however it is possible to gain some insight on the basic parameters of the problem. By introducing the non-dimensional quantities $\bar{r_0} = r_0/l$, $\dot{\bar{r_0}} = \dot{r_0}/U$ and $\dot{\bar{\theta}}_0 = \dot{\theta}_0 l/U$, we obtain,

$$\begin{aligned} \dot{\bar{r_0}} &= -\frac{\Lambda}{\gamma r_0}\tan(\theta_0/\gamma) + \cos(\theta_0-\eta), \\ \dot{\bar{\theta}}_0 &= -\frac{\Lambda}{\bar{r_0}^2} - \frac{\sin(\theta_0-\eta)}{\bar{r_0}}, \end{aligned} \tag{21}$$

where Λ is a non-dimensional parameter, which will be called the *wedge-deflection effect*.

$$\Lambda \equiv \Gamma/(4\pi U l) = v/(4\pi U) \tag{22}$$

In regions with strong circulation or very close to the edge, the velocity field induced by the vortex is dominant and corresponds to large values of Λ. On the contrary, away from the edge or in regions where the vorticity is weak, convection effects are stronger, thus Λ decreases. For instance, at the extreme case when $\Lambda >> 1$ (strong circulation and/or close to the edge and/or very low speed flow) Eq. (21) results asymptotically in the equations of motion obtained in the previous subsection. In the other extreme case when $\Lambda << 1$ (weak circulation and/or far from the edge and/or higher Mach number flow), it yields the equations of motion of a vortex convected by the mean flow. A similar analysis restricted to the case of the half plane was presented by Hardin (1980) in an attempt to model the noise generated by vortices formed at the side edges of flaps [18]. In Hardin's work it is assumed that the vortex is either carried by the potential flow or deflected by the influence of the edge. The former would yield a silent vortex since its path would match with the streamlines of the potential flow around the wedge (as given by Eq. (6)). However, in the present study we are interested in the convection of the vortex by the free stream velocity.

The system of Eqs (20) is solved numerically by implementing a Runge-Kutta scheme of 4^{th} order. Figure 7 shows a comparison of the far field pressure pulse generated by vortices with different wedge effect strengths. It is observed that for large values of Λ the phenomenon evolves very fast and reduces to the problem presented in sub-section III.A. Furthermore, as the wedge-deflection effect decreases, the negative peak of the far-field pressure pulse tends to vanish. This can be explained by the fact that the basic mechanism of sound generation is the crossing of the vortex path with the hypothetical streamlines around the wedge. When convection effects are absent the vortex path is symmetric around the edge and it becomes parallel to the streamlines of the hypothetical potential flow at $\theta_0 = 0$. Then it passes on the lower side of the wedge, where $\theta_0 < 0$. However, when convection effects become important enough, the vortex trajectory changes in a way that it does not become parallel to the hypothetical streamlines and therefore, there is no change of sign. The obtained results can be further investigated by rewriting the far-field pressure signature in the following form.

$$p(r,\theta,\tau) = -\rho_0\sin\left(\frac{\theta}{\gamma}\right) r^{\frac{1}{\gamma}} \frac{\Gamma U}{l^{(1-1/\gamma)}} f(\Lambda,\gamma,\bar{r}_0,\theta_0), \tag{23}$$

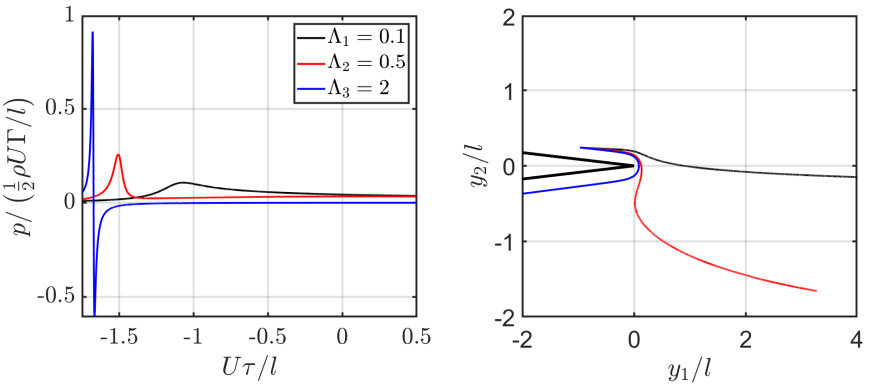

Fig. 7 Influence of parameter Λ on vortex trajectories (right) and far field pressure signature (left). Different vortex paths are shown on the left and the corresponding pressure signatures on the right. The results are shown for $l = 0.01m, U = 30m/s, \Omega = 5^o$ and an observer in the far field $r = 20l$.

where $f\left(\Lambda, \gamma, \bar{r}_0, \theta_0\right)$ corresponds to a function that depends on the trajectory of the vortex around the wedge,

$$f\left(\Lambda, \gamma, \bar{r}_0, \theta_0\right) = \bar{r}_0^{\frac{1}{\gamma}} \left[\frac{\Lambda}{\bar{r}_0^2} \sin\left(\theta_0/\gamma\right) \left(\frac{1-\gamma}{\gamma}\right) - \frac{\cos\left(\eta - \theta_0 \frac{\gamma-1}{\gamma}\right)}{\bar{r}_0} \right] \tag{24}$$

The influence of the main parameters of the problem is more clear in Eqs. (23), (24). The amplitude depends mainly on the flow velocity, the circulation and the length scale that denotes the distance from the edge as is indicated by the factor $\frac{\Gamma U}{l^{(1-1/\gamma)}}$. Further conclusions can be drawn by examining Eq. (24). The function f can be decomposed into two terms, one that corresponds to the influence of the vortex close to the edge and a convection term. We therefore have,

$$f = f_1\left(\Lambda, \bar{r}_0, \theta_0, \gamma\right) + f_2\left(\eta, \bar{r}_0, \theta_0, \gamma\right).$$

When $\bar{r_0}$ is small, the sound pressure field is mainly influenced by $f_1\left(\Lambda, \bar{r}_0, \theta_0, \gamma\right)$. On the contrary as the vortex is convected away from the edge, f_1 decreases as $\bar{r}_0^{\frac{1}{\gamma}-2}$ and convection effects take over ($\bar{r}_0^{\frac{1}{\gamma}-1}$).

C. Application to airfoil noise

We apply the results obtained by the previous analysis to model the far field pressure pulses obtained by turbulent fluctuations impinging on an airfoil with a chord α. The chord is considered to be large enough so that the airfoil edges can be considered separately ($k\alpha >> 1$). The turbulent fluctuations are approximated by point vortices which lie very close to the edges of the airfoil. Hence, the proposed model will be valid when the wavelength (λ) satisfies,

$$l << \lambda << \alpha.$$

Figure 8 depicts the simplified configuration. For purposes of illustration the edges of the airfoil will be approximated

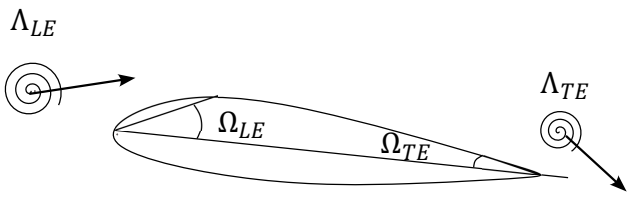

Fig. 8 Simplified configuration for airfoil noise description. The geometry of the airfoil edges is approximated by the wedge angles Ω_{LE} for the leading edge and Ω_{TE} for the trailing edge.

by wedges of different angles. The leading edge is thicker and thus will be modelled with $\Omega_{LE} = 20°$ and the trailing

edge $\Omega_{TE} = 5°$. Furthermore, we assume a mean free-stream flow of $U = 30$m/s, while at the trailing edge it is assumed that the wake velocity is equal to $U_{TE} = 0.7U$, which is a typical wake velocity used in the literature [19], [20]. The initial conditions for the vortex that impinges on the leading edge are

$$r_0 = 3l, \;\; \theta_0 = 0.01\,(\gamma_{LE}\pi)\,,$$

while for the trailing edge

$$r_0 = l, \;\; \theta_0 = -\frac{\gamma_{TE}\pi}{2.1}.$$

The results are shown in Figure 9. It can be seen that the pressure pulse originating from the leading edge is weaker than

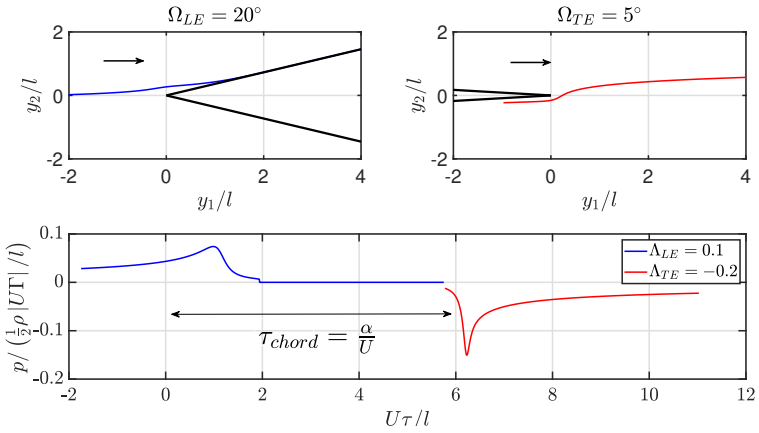

Fig. 9 Leading and trailing edge simulation. The left column in the first row corresponds to a vortex interacting with a leading edge of an airfoil and the arrow shows the direction of the flow. The right column shows the trajectory of a vortex shed at the trailing edge. The plot on the second row depicts the far field pressure pulse obtained by the turbulent fluctuations close to the leading and trailing edge. Results are shown for a mean flow velocity $U_{LE} = 30m/s, U_{TE} = 0.7U, l = 0.01m$ and an observer in the far-field $(r, \theta) = (20l, \pi/2)$.

the one coming from the trailing edge. This result was expected since sharper edges scatter the sound more efficiently. The other important parameter is the strength of the vortex at the airfoil edges. Moreover, the pressure signature of the trailing edge reaches the observer in the far field after $\tau_{chord} = \alpha/U$, which corresponds to the a time delay due to the distance between the leading and trailing edge.

IV. Vortices with finite radius

In the present section, we replace the point vortex with a region of Gaussian vorticity distribution, that is convected with velocity U, passing by the edge of an abritrary semi-infinite rigid wedge. In order to simulate such a flow structure, the Burgers vortex will be used [21]. The velocity and vorticity field are given by the following equations

$$\begin{aligned} \omega_z &= \frac{\Gamma}{2\pi R^2} e^{-\frac{s^2}{2R^2}}, \\ v_\theta &= \frac{\Gamma}{2\pi s}\left(1 - e^{-\frac{s^2}{2R^2}}\right), \end{aligned} \tag{25}$$

where s is a measure of distance from the center of the vortex and R the vortex radius which is used to account for more realistic problems. Since the Burgers vortex is a solution of the flow field that does not take into account the presence of any boundaries, the behavior of the vortex close to the wedge is modeled as follows. It is assumed that the center of the turbulent region translates as a point vortex at velocity $\vec{v}_c$ and, at any instant, an induced velocity field $\vec{v}_\theta$ (Eq. (25)) is added. Therefore, the source term of Howe's acoustic analogy can be split into two terms

$$\vec{\omega}_z \times \vec{v}_c + \vec{\omega}_z \times \vec{v}_\theta.$$

The first term corresponds to a source of sound caused by the displacement of the vortex, while the second one describes an additional source due to the distribution of vorticity in a finite region. A sketch of the problem is depicted in Fig. 10. The equivalent circulation of the center is obtained by

$$\begin{aligned}\Gamma_c &= \int_{R_1}^{R_2}\int_0^{2\pi} \omega_z r dr d\theta,\\ \Gamma_c &= \int_{R_1}^{R_2} \frac{\Gamma}{2\pi R^2} e^{-\frac{s^2}{2R^2}} s ds d\theta,\\ \Gamma_c &= \Gamma\left(1-\frac{1}{\sqrt{e}}\right) \approx 0.39\Gamma.\end{aligned} \tag{26}$$

The motion of the center-point-vortex is described by Equations (20) of Section III. The variables describing the

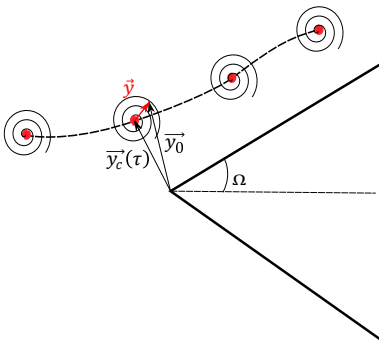

Fig. 10 Region with vorticity distribution close to a wedge. The vector $\vec{y_c}$ is the position vector of the center of the vortex, that changes over time, $\vec{y_0}$ an arbitrary position inside the vortex and $\vec{y} = \vec{y_0} - \vec{y_c}$.

center-point-vortex are denoted with the subscript $(_c)$, i.e. $\Gamma_c, v_{r_c}, v_{\theta_c}$ and the position will be given in polar coordinates at each time instant $(r_c(\tau), \theta_c(\tau))$. The closest distance between the vortex center and the edge is denoted as $l_c = R + l$ where l denotes the closest distance from the finite vortex to the edge. Equation (1) can be expressed as

$$p(r,\theta,t) = \rho_0 \frac{\Gamma}{2\gamma\pi^2 R^2} \frac{\sin(\theta/\gamma)}{r^{\frac{\gamma-1}{\gamma}}} \int_0^{\infty}\int_{-\frac{\gamma\pi}{2}}^{\frac{\gamma\pi}{2}} e^{\frac{-s^2}{2R^2}} r_0^{1/\gamma} \left(-v_{r_c}\cos(\theta_0/\gamma) + \left(v_{\theta_c}+v_\theta\right)\sin(\theta_0/\gamma)\right) d\theta_0 dr_0, \tag{27}$$

where $s = |\vec{y}| = |\vec{y_0} - \vec{y}_c(\tau)|$. It is noted from Eq.(25), $\vec{\omega}_z$ vanishes when the radius of the vortical region tends to zero, that is

$$\lim_{R\to 0} \frac{\Gamma e^{-\frac{s^2}{2R^2}}}{2\pi R^2} = 0.$$

Changing to polar coordinates gives,

$$\begin{aligned}\vec{y_0} &= r_0(\cos\theta_0, \sin\theta_0),\\ \vec{y_c} &= r_c(\cos\theta_c, \sin\theta_c),\\ s^2 &= r_0^2 + r_c^2 - 2r_0 r_c\cos(\theta_0 - \theta_c).\end{aligned} \tag{28}$$

Furthermore, we use the identity

$$-v_{r_c}\cos(\theta_0/\gamma) + v_{\theta_c}\sin(\theta_0/\gamma) = \sqrt{v_{\theta_c}^2 + v_{r_c}^2}\sin\left(\frac{\theta_0}{\gamma} - \tan^{-1}\left(\frac{v_{r_c}}{v_{\theta_c}}\right)\right)$$

Substitution into Eq. (27) leads to

$$p(r,\theta,t) = \rho_0 \frac{\Gamma}{2\gamma\pi^2 R^2} \frac{\sin(\theta/\gamma)}{r^{\frac{\gamma-1}{\gamma}}} (I_1 + I_2)$$

where I_1, I_2 are given by

$$I_1 = \sqrt{v_{\theta_c}^2 + v_{r_c}^2} \int_0^{\infty} \int_{-\frac{\gamma\pi}{2}}^{\frac{\gamma\pi}{2}} r_0^{1/\gamma} e^{-\frac{r_0^2 + r_c^2 - 2r_0 r_c \cos(\theta_0 - \theta_c)}{2R^2}} \sin\left(\frac{\theta_0}{\gamma} - \tan^{-1}\left(\frac{v_{r_c}}{v_{\theta_c}}\right)\right) d\theta_0 dr_0 \tag{29}$$

$$I_2 = \int_0^{\infty} \int_{-\frac{\gamma\pi}{2}}^{\frac{\gamma\pi}{2}} \frac{\Gamma r_0^{1/\gamma} \sin(\theta_0/\gamma)}{2\pi\sqrt{r_0^2 + r_c^2 - 2r_0 r_c \cos(\theta_0 - \theta_c)}} \left(e^{-\frac{r_0^2 + r_c^2 - 2r_0 r_c \cos(\theta_0 - \theta_c)}{2R^2}} - e^{-\frac{r_0^2 + r_c^2 - 2r_0 r_c \cos(\theta_0 - \theta_c)}{R^2}}\right) d\theta_0 dr_0 \tag{30}$$

The integrals of Eqs. (29),(30) are non-dimensionalised in the same way as presented in Section III.B Equations (29), (30) become

$$I_1 = U l^{\frac{\gamma+1}{\gamma}} e^{-\frac{l^2}{R^2}} \sqrt{\bar{r}_c^2 \dot{\bar{\theta}}_c^2 + \dot{\bar{r}}_c^2} \int_0^{\infty} \int_{-\frac{\gamma\pi}{2}}^{\frac{\gamma\pi}{2}} \bar{r}_0^{1/\gamma} e^{-\frac{\bar{r}_0^2 + \bar{r}_c^2}{2}} e^{\bar{r}_0 \bar{r}_c \cos(\theta_0 - \theta_c)} \sin\left(\frac{\theta_0}{\gamma} - \tan^{-1}\left(\frac{\dot{\bar{r}}_c}{\bar{r}_c \dot{\bar{\theta}}_c}\right)\right) d\theta_0 d\bar{r}_0 \tag{31}$$

$$I_2 = \Gamma l^{\frac{1}{\gamma}} e^{-\frac{l^2}{R^2}} \int_0^{\infty} \int_{-\frac{\gamma\pi}{2}}^{\frac{\gamma\pi}{2}} \frac{\bar{r}_0^{1/\gamma} \sin(\theta_0/\gamma) \left(e^{-\frac{\bar{r}_0^2 + \bar{r}_c^2 - 2\bar{r}_0 \bar{r}_c \cos(\theta_0 - \theta_c)}{2}} - e^{-\bar{r}_0^2 - \bar{r}_c^2 + 2\bar{r}_0 \bar{r}_c \cos(\theta_0 - \theta_c)}\right)}{2\pi\sqrt{\bar{r}_0^2 + \bar{r}_c^2 - 2\bar{r}_0 \bar{r}_c \cos(\theta_0 - \theta_c)}} d\theta_0 d\bar{r}_0 \tag{32}$$

As a result, the far field pressure pulse depends o the main parameters of the problem as follows

$$p \sim \left(\Gamma U l I_1(\Lambda) + \Gamma^2 I_2\right) \frac{l^{\frac{1}{\gamma}} e^{-\frac{l^2}{R^2}}}{R^2}. \tag{33}$$

The influence of the vorticity region R becomes clearer if we write

$$R = l\beta$$

where β is the magnitude by which R is bigger or smaller than l. Eq. (33) then becomes,

$$p \sim \left(\Gamma U l I_1(\Lambda) + \Gamma^2 I_2\right) \frac{l^{\left(\frac{1}{\gamma} - 2\right)} e^{-\frac{1}{\beta^2}}}{\beta^2}, \tag{34}$$

The effect of the vortex radius becomes more apparent by the results shown in Figure 11. The far field pressure pulse induced by a vortex motion close to a half-plane is plotted for different vortex radii and compared against the results obtained by modelling the same problem with a point vortex. For vortices concentrated in a region $R < l$ or $R > l$ the far-field pressure pulse tends to be weaker. However, for $R = l$ the far field pressure signature takes its maximum value. It can be observed that by keeping the distance between the vortex and the edge constant, the distance between the edge and the vortex center grows for higher radii. As a result, larger vortices yield a weaker and smoother acoustic pressure signature in comparison to the point vortex.

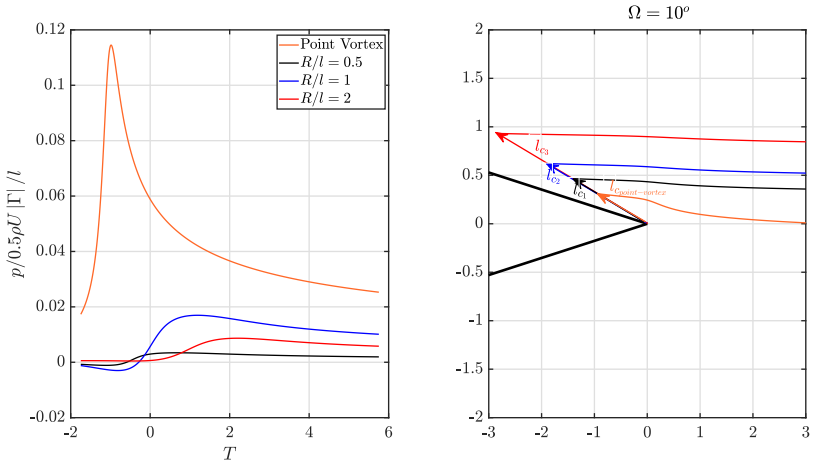

Fig. 11 Far field pressure pulse for vortices with different diameters for a wedge angle of $\Omega = 10^o$, $U = 40m/s$, $\Gamma = 2Ul$, $l = 0.01$ and the observer lies in the far field at $r = 20l$. The right plot shows the trajectory of the center of the finite vorticity regions, for different values of the radius R.

V. Conclusions

We studied the aerodynamic sound induced by turbulent fluctuations, modelled as point vortices, interacting with a rigid semi-infinite wedge. The present work extends the simplified model for sound generation by a point vortex close to a semi-infinite, rigid half-plane, which was first presented by Crighton (1972) [10] and then treated by Howe, details shown in [7], [12],[13]. A closed form analytical expression for the far-field acoustic pulse has been obtained, when a point vortex is deflected by an edge with arbitrary angle 2Ω. Further analysis of the model resulted in scaling laws, that illustrate the dependence of the acoustic pressure on the distance between the edge and the vortex. A comparison was done with the theoretical and experimental work of Kambe et al. [14]. Furthermore, convection effects due to the free-stream flow have been taken into account, and it was shown that there exists a non-dimensional parameter, called the wedge-deflection effect, which drives the kinematics of the vortex close to the edge of the semi-infinite rigid wedge. Further analysis has shown:

- the larger the wedge angle the weaker the far field pressure pulse
- Increase of the wedge angle leads to shorter radiation times
- Convection effects influence strongly the far-field pressure signature (Fig. 7)
- While the vortex lies close to the edge, sound is mainly produced due to the deflection of the vortex path by the edge, while for vortices further away from the edge, convection effects take over and weaker acoustic pressure pulse is obtained.

The presented work has been compared with similar studies in the literature and the following conclusions can be drawn: i) the description of the kinematics of the vortex close to the wedge combines the assumptions used by Howe (2002) (self induction of the vortex by its image point at the edge) and by Kambe et al. (1985) (pure convection of the vortex with the mean flow), ii) the current model can be used to describe general edge noise problems, such as leading/trailing edge noise, or the noise generated by vortices at the side edges of the flaps [18], [22]. Furthermore, an application to airfoil noise was shown, where the airfoil edges where modelled by semi-infinite wedges. Finally, the point vortex was replaced by a vorticity region with Gaussian distribution of vorticity around its center. A vortex radius was used to account for more realistic problems and it was shown that larger regions of vorticity distribution tend to smooth and weaken the far field pressure pulse.

Acknowledgements

This work was supported by the DGAC (Direction Générale de l'Aviation Civile), by the PNRR (Plan National de Relance et de Résilience Français) and by NextGeneration EU via the project MAMBO (Méthodes Avancées pour la Modélisation du Bruit moteur et aviOn.

References

[1] Zhao, K., Okolo, P., Neri, E., Chen, P., Kennedy, J., and Bennett, G. J., "Noise reduction technologies for aircraft landing gear-A bibliographic review," *Progress in Aerospace Sciences*, Vol. 112, 2020, p. 100589.

[2] Lee, S., Ayton, L., Bertagnolio, F., Moreau, S., Chong, T. P., and Joseph, P., "Turbulent boundary layer trailing-edge noise: Theory, computation, experiment, and application," *Progress in Aerospace Sciences*, Vol. 126, 2021, p. 100737.

[3] Lighthill, M. J., "On sound generated aerodynamically I. General theory," *Proceedings of the Royal Society of London. Series A. Mathematical and Physical Sciences*, Vol. 211, No. 1107, 1952, pp. 564–587.

[4] Curle, N., "The influence of solid boundaries upon aerodynamic sound," *Proceedings of the Royal Society of London. Series A. Mathematical and Physical Sciences*, Vol. 231, No. 1187, 1955, pp. 505–514.

[5] Williams, J. F., and Hawkings, D. L., "Sound generation by turbulence and surfaces in arbitrary motion," *Philosophical Transactions for the Royal Society of London. Series A, Mathematical and Physical Sciences*, 1969, pp. 321–342.

[6] Powell, A., "Theory of vortex sound," *The journal of the acoustical society of America*, Vol. 36, No. 1, 1964, pp. 177–195.

[7] Howe, M., "Contributions to the theory of aerodynamic sound, with application to excess jet noise and the theory of the flute," *Journal of Fluid Mechanics*, Vol. 71, No. 4, 1975, pp. 625–673.

[8] Williams, J. E. F., and Hall, L. H., "Aerodynamic sound generation by turbulent flow in the vicinity of a scattering half plane," *Journal of Fluid Mechanics*, Vol. 40, No. 4, 1970, p. 657–670. https://doi.org/10.1017/S0022112070000368.

[9] Crighton, D., and Leppington, F., "On the scattering of aerodynamic noise," *Journal of Fluid Mechanics*, Vol. 46, No. 3, 1971, pp. 577–597.

[10] Crighton, D. G., "Radiation from vortex filament motion near a half plane," *Journal of Fluid Mechanics*, Vol. 51, No. 2, 1972, p. 357–362. https://doi.org/10.1017/S0022112072001235.

[11] Howe, M. S., "The generation of sound by aerodynamic sources in an inhomogeneous steady flow," *Journal of Fluid Mechanics*, Vol. 67, No. 3, 1975, p. 597–610. https://doi.org/10.1017/S0022112075000493.

[12] Howe, M. S., *Sound generation in a fluid with rigid boundaries*, Cambridge Monographs on Mechanics, Cambridge University Press, 1998, p. 157–252. https://doi.org/10.1017/CBO9780511662898.004.

[13] Howe, M. S., *Theory of Vortex Sound*, Cambridge Texts in Applied Mathematics, Cambridge University Press, 2002. https://doi.org/10.1017/CBO9780511755491.

[14] Kambe, T., Minota, T., and Ikushima, Y., "Acoustic wave emitted by a vortex ring passing near the edge of a half-plane," *Journal of Fluid Mechanics*, Vol. 155, 1985, pp. 77–103.

[15] Chang, C.-C., and Chen, T.-L., "Acoustic emission by a vortex ring passing near a sharp wedge," *Proceedings of the Royal Society of London. Series A: Mathematical and Physical Sciences*, Vol. 445, No. 1923, 1994, pp. 141–155.

[16] Priddin, M., Baker, D. I., Ayton, L. J., and Peake, N., "Vortex sound models: passive and active noise control," *2018 AIAA/CEAS Aeroacoustics Conference*, 2018, p. 3298.

[17] Howe, M. S., *Vortex–Surface Interaction Noise in Two Dimensions*, Cambridge Texts in Applied Mathematics, Cambridge University Press, 2002, p. 136–155. https://doi.org/10.1017/CBO97805117554910.007.

[18] Hardin, J. C., "Noise radiation from the side edges of flaps," *AIAA Journal*, Vol. 18, No. 5, 1980, pp. 549–552.

[19] Howe, M. S., "A review of the theory of trailing edge noise," *Journal of sound and vibration*, Vol. 61, No. 3, 1978, pp. 437–465.

[20] Moreau, S., and Roger, M., "Back-scattering correction and further extensions of Amiet's trailing-edge noise model. Part II: Application," *Journal of Sound and vibration*, Vol. 323, No. 1-2, 2009, pp. 397–425.

[21] Burgers, J. M., "A mathematical model illustrating the theory of turbulence," *Advances in applied mechanics*, Vol. 1, 1948, pp. 171–199.

[22] Roger, M., Moreau, S., and Kucukcoskun, K., "On sound scattering by rigid edges and wedges in a flow, with applications to high-lift device aeroacoustics," *Journal of Sound and Vibration*, Vol. 362, 2016, pp. 252–275.

A. Vortex around a semi-infinite wedge (convection effects neglected)

In this appendix the derivation of the vortex path and the far field pressure signature of Eqs.(9), (10) is presented. The velocity, obtained by the complex velocity potential is written as

$$\frac{d\bar{z}_0}{d\tau} = -i\frac{\Gamma\zeta''(z_0)}{4\pi\zeta'(z_0)} + \frac{d}{dz_0}\left[\frac{i\Gamma}{2\pi} ln\left(\zeta(z) - \zeta(\bar{z}_0)\right)\right] \tag{A.1}$$

Substituting

$$\zeta(z_0) = iz_0^{1/\gamma} = ir_0^{1/\gamma} e^{i\theta_0/\gamma}$$

it yields:

$$\begin{aligned}\frac{d}{d\tau}\{r_0\cos\theta_0 - ir_0\sin\theta_0\} &= \frac{\Gamma}{4\pi\gamma r_0}\left[(\gamma-1)\sin\theta + \frac{\sin\left(\theta_0\frac{\gamma-1}{\gamma}\right)}{\cos\left(\frac{\theta_0}{\gamma}\right)}\right] \\ &+\frac{i\Gamma}{4\pi\gamma r_0}\left[(\gamma-1)\cos\theta + \frac{\cos\left(\theta_0\frac{\gamma-1}{\gamma}\right)}{\cos\left(\frac{\theta_0}{\gamma}\right)}\right]\end{aligned} \tag{A.2}$$

By taking the derivative in time and separating the real and imaginary parts of the complex number, the following system of Equations is obtained:

$$\begin{pmatrix}\cos\theta_0 & -r_0\sin\theta_0 \\ \sin\theta_0 & r_0\cos\theta_0\end{pmatrix}\frac{d}{d\tau}\begin{pmatrix}r_0 \\ \theta_0\end{pmatrix} = \begin{pmatrix}\frac{\Gamma(\gamma-1)}{4\pi\gamma r_0}\sin\theta_0 + \frac{\Gamma}{4\pi\gamma r_0}\frac{\sin\left(\theta_0\frac{\gamma-1}{\gamma}\right)}{\cos(\theta_0/\gamma)} \\ \frac{-\Gamma(\gamma-1)}{4\pi\gamma r_0}\cos\theta_0 - \frac{\Gamma}{4\pi\gamma r_0}\frac{\cos\left(\theta_0\frac{\gamma-1}{\gamma}\right)}{\cos(\theta_0/\gamma)}\end{pmatrix} \tag{A.3}$$

The solution of Eq.(A.3) is obtained by the method of determinants and the following trigonometric relations are used

$$\cos x\sin y - \sin x\cos y = -\sin(x-y)$$

$$\cos x\cos y + \sin x\sin y = -\cos(x-y)$$

It follows

$$\frac{dr_0}{d\tau} = -\frac{\Gamma}{4\pi\gamma r_0}\tan(\theta/\gamma) \tag{A.4}$$

$$\frac{d\theta_0}{d\tau} = -\frac{\Gamma}{4\pi r_0^2} \tag{A.5}$$

From (A.5),(A.4) it follows

$$r_0\frac{d\theta_0}{dr_0} = \gamma\cot\left(\frac{\theta_0}{\gamma}\right) \tag{A.6}$$

which leads to

$$\int \gamma^{-1}\tan(\theta_0/\gamma)\,d\theta_0 = \int r_0^{-1}dr_0 \Rightarrow r_0 = l\sec(\theta_0/\gamma) \tag{A.7}$$

Then, substituting Eq. (A.7) into (A.5) and following Howe's notation it yields

$$\begin{aligned}r_0(\tau) &= l\sqrt{1+(2\tilde{\tau}/\gamma)^2} \\ \theta_0(\tau) &= \gamma\tan^{-1}(-2\tilde{\tau}/\gamma),\end{aligned} \tag{A.8}$$

where $\tilde{\tau} = (\tau\Gamma)/\left(8\pi l^2\right)$. Furthermore by combining Eqs. (A.8) and Eq.(7) and using the identities

$$\cos\left[\tan^{-1}x\right] = \left(x^2+1\right)^{-1/2}$$

$$\sin\left[\tan^{-1}(-x)\right] = -\frac{x}{\sqrt{x^2+1}}$$

we result in Eq. (10).